Fifth International Conference on Construction in the 21st Century (CITC-V)
"Collaboration and Integration in Engineering, Management and Technology"
May 20-22, 2009, Istanbul, Turkey

Experimental and Numerical Investigations of Steel Tension Members with Holes

P. Arasaratnam
Department of Civil Engineering, McMaster University, Hamilton, ON, CANADA

M. Tait
Department of Civil Engineering, McMaster University, Hamilton, ON, CANADA

K.S. Sivakumaran
Department of Civil Engineering, McMaster University,
Hamilton, Ontario, CANADA, L8S 4L7
siva@mcmaster.ca

Abstract
This paper discusses the experimental and numerical investigations conducted on steel tension members, in order to develop appropriate material stress-strain relationship for numerical analysis, which can capture the behaviour of structural steel including the fracture. Twenty eight tensile coupons were obtained from beam sections made of two different steel grades; ASTM A992 steel and 350W steel. The test program considered flange and web coupons, both solid and perforated samples (Net area-to-gross area A_n/A_g ratio 0.9 to 0.5) having different diameter holes in the middle region. The experiments on solid coupons provided the engineering stress-strain relationships until fracture. These relationships were converted to true stress - true strain relations up to ultimate strength. A unique material constitutive relation for post-ultimate region, which is expected to capture the behaviour of the coupons up to fracture, was derived by simulating these tests using Finite Element (FE) analyses. This material constitutive relation so derived was then used to predict the load-deformation behaviour of coupons with a hole in the middle region subjected to direct tension loading. The FE predictions for perforated tension coupons agreed well with the corresponding experimental results.

Keywords
Steel tension coupons, Experimental investigation, Stress-strain relations, Holes, Finite Element analysis

1. Introduction

Steel structures construction often necessitates fabrication of holes in the flanges of steel beams. Even though the current Canadian Steel Design Code- Clause 14.1 (CSA, 2003) gives guidance on the flexural strength beams having flange holes, over the years the steel properties and the related international design provisions have changed. Recently, a research project considered the effects of flange holes on the flexural behaviour of steel I-beams, which indicated that the beams having smaller holes failed due to flange buckling, whereas the beams having larger tension flange holes failed due to fracture. These experimental results can be effectively expanded through finite element (FE) analyses; however, such FE models require realistic material stress-strain relationships, which can capture the fracture of steel as well.

This paper discusses the experimental and numerical investigations conducted on solid, as well as perforated, steel tension members to establish such material models for the behaviour of structural steel.

2. The Experimental Program

The test program considered two different steel grades namely; ASTM A992 steel and the 350W steel. The A992 steel grade is now widely used in North America. The 350W steel is the Canadian standard CSA G40.21 (CISC, 2007) steel, which is equivalent to ASTM A572 Grade 50 steel. The tensile coupons were cut along the rolling direction of the W310X39 (W12X26) wide flange beam sections. The dimensions of the tensile coupons were in accordance with ASTM A370-02 (ASTM, 2002) specifications and recommendations. The average width and the average thickness of the test coupons were established based on several measurements taken within the reduced cross-section of the coupons and the initial cross-sectional area of each specimen was calculated based on these measured dimensions. Eight flange coupons and six web coupons were obtained for each steel grade. Three identical flange solid coupons and three identical web solid coupons were used to establish the mechanical characteristics of these two steel grades. The five remaining flange coupons and the three remaining web coupons were used as perforated tension coupons having different diameter holes at the centre of the specimens. These samples had the net area-to-gross area A_n/A_g ratio ranging from 0.9 to 0.5 in increments of 0.1. Holes with A_n/A_g ratios of 0.9, 0.7 and 0.5 were considered for the web coupons. Figure 1 shows some of these test coupons.

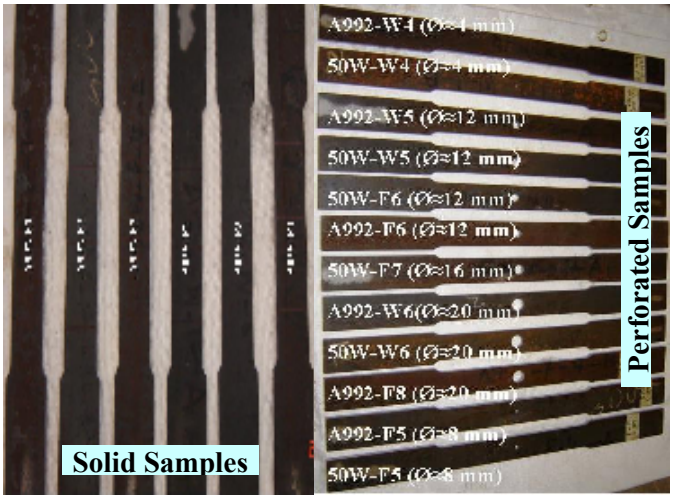

Figure 1: The Tensile Test Coupons

The tension tests were performed using a Tinius Olsen machine with an axial load capacity of 600 kN. Each test specimen was first aligned vertically and placed at the center position with respect to the grips of the machine's loading platforms. First a cycle of low load was applied to permit proper grip of the test specimen in the machine. Two extensometers having gauge lengths of 200 mm and 50 mm, respectively, were attached on either face of the test coupon. The larger extensometer was used to establish the overall engineering stress-strain curve of the coupon, whereas the smaller extensometer assisted with the establishment of the initial modulus E and the proportional limit F_{pl}. The coupons were tested at a loading rate of 0.5 mm/min in the elastic range. The loading rate was, however, increased to 2.5 mm/min in the strain-hardening range up to the ultimate loads. Beyond the ultimate loads, the loading rate was reduced to 0.5 mm/min up to fracture (Jaquess and Frank, 1999). A lower loading rate was applied in the strain softening region in order to minimize the influence of strain rate on the fracture. Previous studies have clearly shown that higher strain rates result in lower fracture strains (Liu, 2005).

Figure 2 shows the experimental engineering stress - engineering strain relationships of the solid tensile coupons obtained from the flanges and webs of the A992 steel section. The average yield strength F_y and average ultimate strength F_u of the A992-flange coupons were calculated to be 445 MPa and 577 MPa, respectively, resulting in the F_y/F_u ratio of 0.77. The strains corresponding to the ultimate strength ε_u and at fracture ε_f were measured to be 13.8% and 21%, respectively. The 350W-flange coupons had the F_y and F_u values of 428 MPa and 578 MPa, respectively, resulting in the F_y/F_u ratio of 0.74. The ε_u and ε_f values associated with these coupons were 13.9% and 22%, respectively. The F_y/F_u ratio value for the A992-flange coupon was 4% higher than that of the 350W-flange coupon. The F_y and F_u values for the A992-web coupons were 409 MPa and 573 MPa, respectively, resulting in the F_y/F_u ratio value of 0.71. These coupons reached the ultimate strength at the strain of 14.5% and fractured at the strain of 21%. The 350W-web coupons had the F_y and F_u values of 416 MPa and 582 MPa, respectively, resulting in the F_y/F_u ratio value of 0.71. These coupons had ε_u and ε_f of 15.3% and 19.5%, respectively.

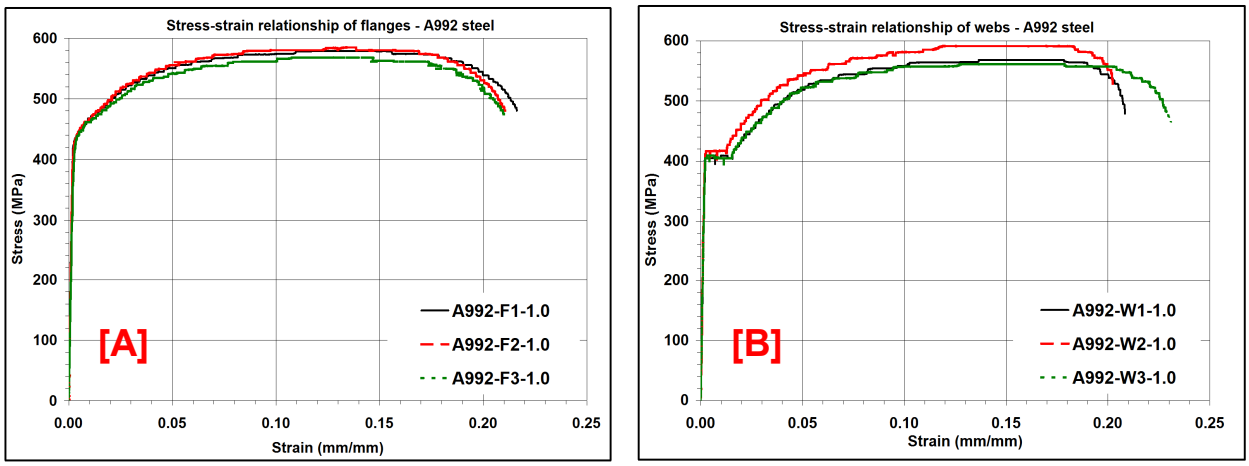

Figure 2: Sample Stress-Strain Relations – A992 Steel Grade [A] Flange [B] Web

The behaviour of tension members with holes is considerably different when compared to the behaviour of similar solid members having uniform cross-section. The experimental stress-strain behaviours of tension coupons with holes are given in a later section of this paper. Tension members having holes are non-uniformly stressed due to the stress concentration effects in the vicinity of hole region. The presence of small local holes in a tension member (such as small bolt holes used for the connection of the member) causes early yielding around the holes so that the load-deflection relations exhibit early non-linear behaviour. When holes are small compared to the gross cross-section, the member may reach the gross-section yield load A_gF_y. On the other hand, when holes are large, the member may fail due to fracture, prior to reaching the A_gF_y. Therefore, for yielding to occur in the gross area before fracturing through the net area, it is necessary that $A_nF_u > A_gF_y$ or $A_n > Y\ A_g$, where Y is the yield ratio F_y/F_u. It can be stated then that for members of the same geometry with the same hole size, the yield ratio determines whether the gross area yields before fracture of the net area.

Table 1 summarizes the measured ultimate load P_u, the P_u/P_y ratio values, the peak average stress across the net-section $F_{un} = P_u/A_n$ and the strength ratios between the coupons having a middle hole and the solid samples F_{un}/F_u. It can be noted that the coupons having the $A_nF_u/A_gF_y>1.0$ reached an ultimate load higher than $P_y=A_gF_y$. The coupons with the $A_nF_u/A_gF_y<1.0$ fractured prior to reaching P_y. Furthermore, as summarized in the ninth column of this table, the ultimate strengths of perforated samples F_{un} were between 2% - 8% higher than the ultimate strength of solid samples. A similar observation was made by Fisher (1965). He explained that when holes occur in an axial tension member a free lateral contraction accompanying an axial extension cannot develop. This may result in a slightly higher strength for perforated samples when compared to that of the solid samples (Fisher, 1965). The strength ratios had no

definite pattern. This may be due to various factors such as variations in material properties, geometric imperfections, hole making practices, etc. (Fisher, 1965).

Table 1: Analysis of the Strength of Tension Members with Holes

Steel Grade	Specimen ID	Hole Diameter-φ (mm)	$\left[A_n / A_g\right]$ (%)	$\left[A_n F_u / A_g F_y\right]$	Ultimate Load P_u (kN)	$\left[\frac{P_u}{P_y}\right]$ $(P_y = A_g F_y)$	Ultimate Stress-F_{un} (MPa)	Strength Ratio $\left[\frac{F_{un}}{F_u}\right]$
(1)	(2)	(3)	(4)	(5)	(6)	(7)	(8)	(9)
A992 (Flange) $[F_y = 445MPa$ $F_u = 577MPa]$	**A992-F-0.9**	4.06	90	**1.17>1.0**	215.5	**1.24**	613	1.06
	A992-F-0.8	8.03	80	**1.04>1.0**	170.0	**1.09**	608	1.05
	A992-F-0.7	12.07	70	0.91<1.0	147.8	0.97	615	1.06
	A992-F-0.6	16.05	60	0.78<1.0	145.0	0.83	619	1.07
	A992-F-0.5	19.94	50	0.65<1.0	106.5	0.69	612	1.06
A992 (Web) $[F_y = 409MPa$ $F_u = 573MPa]$	**A992-W-0.9**	4.04	90	**1.26>1.0**	121.2	**1.29**	587	1.02
	A992-W-0.7	12.07	70	0.98≈1.0	97.5	**1.03**	604	1.05
	A992-W-0.5	20.02	50	0.70<1.0	70.0	0.74	602	1.05
350W (Flange) $[F_y = 428MPa$ $F_u = 578MPa]$	**350W-F-0.9**	4.09	90	**1.22>1.0**	190.0	**1.29**	614	1.06
	350W-F-0.8	8.03	80	**1.08>1.0**	195.5	**1.14**	612	1.06
	350W-F-0.7	12.07	70	0.94<1.0	170.2	0.99	608	1.05
	350W-F-0.6	16.33	59	0.80<1.0	127.0	0.86	621	1.08
	350W-F-0.5	19.99	50	0.68<1.0	122.0	0.72	615	1.07
350W (Web) $[F_y = 416MPa$ $F_u = 582MPa]$	**350W-W-0.9**	4.09	90	**1.26>1.0**	122.3	**1.29**	595	1.02
	350W-W-0.7	12.07	70	0.98≈1.0	96.5	**1.01**	602	1.03
	350W-W-0.5	19.89	50	0.70<1.0	69.0	0.72	591	1.02

3. Development of a Material Model

In general, a standard uni-axial tensile test provides the basic tensile properties of a material, particularly in the range of small elastic-plastic deformations. In tensile testing, however, in general the uniform extension ceases when the load exceeds the peak load P_u (tensile strength F_u). Beyond this limit, the material appears to strain soften due to necking of the sample, and due to the use of original cross-sectional area in stress calculations. Once the specimen begins to 'neck', the distribution of stresses and strains become complex and the magnitude of such quantities become difficult to establish (Mackenzie et al., 1977). Owing to the non-uniform stress and strain distributions existing at the neck for high levels of axial deformation, it has long been recognized that the significant changes in the geometric configurations of the specimen have to be considered to properly describe the material response during the whole deformation process up to the fracture (Cabezas et al, 2003). The constitutive model requires the true stress-strain curve of the material in order to carry out the numerical analysis. The true stress versus the true strain relationship can be established directly from the engineering stress versus the engineering strain relationship using $F_t = F_e(1+ \varepsilon_e)$ and $\varepsilon_t=\ln(1+ \varepsilon_e)$, where F_t is the true stress, ε_t is the true strain and where F_e is the engineering stress and ε_e is the engineering strain. The above relations between true and engineering quantities are based on two assumptions; (1) the stresses are uniform across the specimen and (2) material flows with negligible volume change. Since the stresses are no longer uniformly distributed over a gauge length beyond the onset of necking these equations are invalid in the post ultimate range.

Figure 3 shows the engineering stress – engineering strain relationship that is characteristic of many steels for structural applications, and the true stress – true strain relationships (dash-line in Figure 3). These relationships can be divided into five different regions as follows;

- Region-I (elastic range): during the initial stages of loading, stress varies linearly proportional to the strain (up to a proportional limit). The stress at the proportional limit is typically established using the 0.01% strain offset method. Thus, the stress can be related to strain as $F_e = E\ \varepsilon_e$ in the range $F_e < F_{pl}$ and E is the initial elastic modulus. Also, $F_t = F_e(1+ \varepsilon_e)$ and $\varepsilon_t=\ln(1+ \varepsilon_e)$.

- Region-II: represents a region from the proportional limit to the yield limit. In this region, the variation of stress-strain relationship can be idealized as $F_e = E_t \varepsilon_e$, which is valid in the range $F_{pl} < F_e < F_y$. E_t is the tangent modulus $E_t = (F_y - F_{pl})/(\varepsilon_y - \varepsilon_{pl})$. Also, $F_t = F_e(1+\varepsilon_e)$ and $\varepsilon_t = \ln(1+\varepsilon_e)$.
- Region-III: after the initiation of yielding, there may be a yield plateau, and the stress in this region is assumed to be constant of F_y, which is valid in the range $\varepsilon_y < \varepsilon_e < \varepsilon_{sh}$, where ε_{sh} is the strain at the onset of hardening. The ratio between ε_{sh} and ε_y may be defined as $m = \varepsilon_{sh} / \varepsilon_y$.
- Region-IV: at the end of yield plateau, strain hardening begins, with a subsequent increase in strength. Region-IV includes the strain hardening range up to ultimate strength when the test specimen may begins to exhibit necking. Though this region involves a non-linear stress-strain relation, the true stress and the true strain can be obtained using the relations $F_t = F_e(1+\varepsilon_e)$ and $\varepsilon_t = \ln(1+\varepsilon_e)$. A power-law is often used to relate the true stress – true strain relationship in the strain hardening region (Holloman, 1945 and Bruneau et al., 1998). In this study, a power law of the form $F_t = F_{ut} (\varepsilon_t/\varepsilon_{ut})^n$ was considered, where F_{ut} and ε_{ut} are the true stress and true strain associated with ultimate tensile strength F_u. The value for n was established for different steel grades and for flange and web using a least square analysis of the corresponding experimental results. Figure 4 shows the true stress – true strain relationship in Regions I, II, III & IV (Power Law), derived for A992-Flange specimen test results shown in Figure 2 [A].
- Region-V: represents the post ultimate strength behaviour of the material. Associated behaviour is complex and true stress-strain relations and the fracture strains are not easy to establish. As explained below, in this study, an experimental-numerical iterative approach was used. Zhang et al. (1994) proposed that the parameters for a true stress-true strain relation be determined using iterative Finite Element Method based analyses and using an experimental tensile load-extension curve as a target. Though true stress and true strain are established without dimensional measurements during the test, the main short coming of this method is that the entire stress-strain relation during necking is treated as unknown and a trial and error procedure is used for a series of strain intervals until good correlation with the experimental results is attained. Thus, Zhang et al. (1994) proposed method is computationally intensive and time-consuming. Ling (1996) proposed a weighted-average method for determining uni-axial true stress versus true strain relation during necking. This method requires identification of a lower and an upper bound for the true stress-strain function during necking and expresses the true stress-strain relation as the weighted average of these two bounds. According to Ling (1996) a power-law fit, which represents strain hardening region of the flow curve, can be used as the lower bound, whereas a linear hardening model can be used as the upper bound. Figure 4 shows these upper and lower bound models and the weighted model. $F_t = (a_0 + a_1 \varepsilon_t)$ could be the linear hardening model, where constants $a_0 = F_{ut}(1 - \varepsilon_{ut})$ and $a_1 = F_{ut}$. Based on the weighted average method, the true stress-strain relation in the post ultimate strength region (Region-V) may be related as $F_t = F_{ut}[w.(\varepsilon_t/\varepsilon_{ut})^n + (1-w).(1+\varepsilon_t - \varepsilon_{ut})]$, where w is the unknown weighting constant. A suitable weight constant has to be established in an iterative manner by numerical simulation of tensile test until a good correlation is achieved between the calculated and the experimental load extension curve.

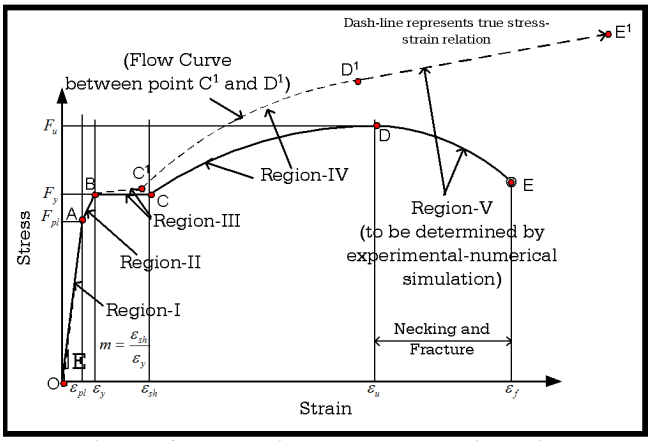

Figure 3: Material Models: Engineering Stress-Strain and True Stress-Strain Relations

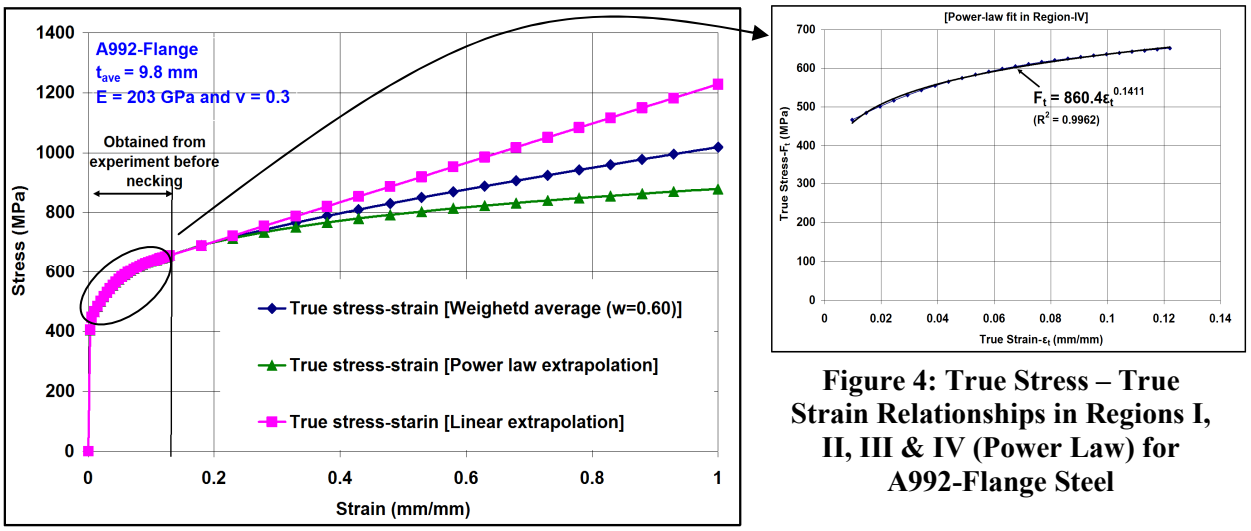

Figure 4: True Stress – True Strain Relationships in Regions I, II, III & IV (Power Law) for A992-Flange Steel

3.1 Finite Element Models

In the numerical simulation, the tensile test coupon was modeled using 4-node shell elements with six degree of freedom per node. This element can be employed to model thick and thin general shell structures and it accounts for finite strains by allowing for changes in the element thickness (Bathe, 1996). Also, this shell element can be efficiently used with plastic multi-linear material models for large-displacement/large-strain analyses (Cabezas et al., 2004). The shell elements had 2x2 integration points in the mid surface (in r-s plane) and 3 Gauss numerical integration points through thickness (in t-direction). The model also incorporated a geometric imperfection (Maximum amplitude of 0.1% of the width-40 mm) of a half sine wave along the gauge length in order to cause diffuse necking. The analysis incorporated both geometric and material non-linearities (von Mises yield criterion and isotropic hardening rule). One edge of the model was fully restrained while the other end was subjected to a uniform displacement. For members with mid-hole, a fine mesh was used for a 50 mm length of the mid-sample where the strain gradient is expected to be large. Up to ultimate strength (Regions I, II, III & IV) the true stress and strain relationship was derived from the engineering stress - strain curve obtained from tension coupon tests. The material model in Region V, however, needed an additional point E^1 as shown in Figure 3, even though the true stress – true strain relation for Region V could be established using the weighted average method. Study by Khoo (2000) indicated that the localized fracture strains for structural steel under uni-axial tensile load could vary between 80% and 120%. The estimated fracture strain ε_{ft} associated with the experimental results shown in Figure 2 ranged 65% - 75%. In this study, the true strain at point E^1 was taken as ε_{ft} = 100%. For comparison purposes, Figure 5 shows the photograph of a test specimen after failure, and corresponding finite element models.

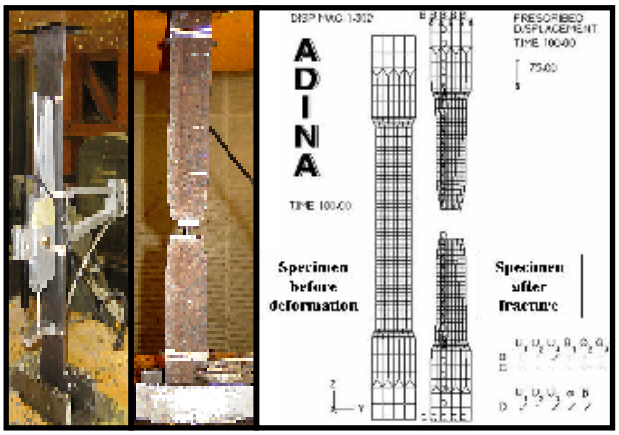

Figure 5: Comparison of Failure Pattern of Test Sample with FE Simulation Results

The weighting constant w for Region V has to be established in an iterative manner by numerical simulation of tensile tests until a good correlation is achieved between the calculated and the experimental load extension curves. In order to illustrate the influence of the weighting constant, three different values for w = 1.0, 0.6 and 0.4 were considered in the numerical simulations. Figure 6 shows the resulting FEM-predicted responses along with the experimental responses of three identical tension coupons (A992-flange). The weighting factor w=1.0, which represents the Region-V by a power-law hardening model, results in a numerical response well below the experimental curve. However, for w=0.4, the numerical curve was slightly above the experimental curve. The weighting value w=0.6 appears to give the best fit for this set of experimental results. Although a suitable weight constant w to reproduce the experimental stress-strain curve needs to be established by trial and error approach, only a few trials were required in this study.

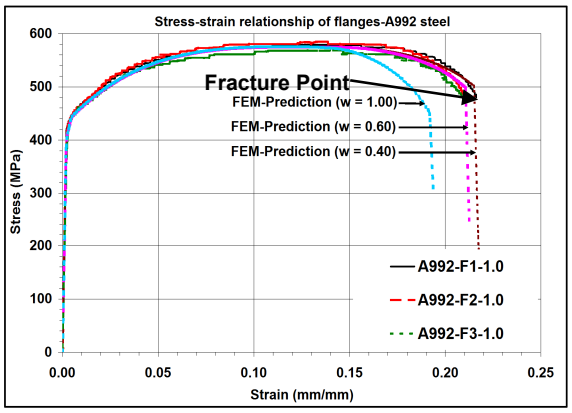

Figure 6: Influence of Weighting Constant

In summary, the procedural steps associated with the development of the material model for numerical analysis of steel until fracture are as follows; [1] establish the pre-strain-hardening true stress-strain curve directly from the experimentally obtained engineering stress-strain curve. [2] use a power-law model fit to the true stress-strain curve in the strain hardening range (Region-IV). [3] extrapolate the true stress-strain relation for Region V, using a weighting factor and using the power-law model (established for Region IV) and a linear model. [4] perform numerical simulations with the true stress-strain curve obtained in previous steps and using different weighting constants, until the relative error between the resulting numerical stress-strain relations and the corresponding experimental responses are minimized. Table 2

summarizes the power models and the weighting constants derived for A992 steel grade and for 350W steel grade. Experimental results corresponding to three identical flange coupons and three identical web coupons were considered in the derivation of these model parameters. Based on the FE simulation of tensile tests in this study, the weighting constants w=0.6 and w=0.5 were close enough to reproduce the stress-strain curve established from the flanges and webs of both ASTM A992 steel and 350W steel grades, respectively. Numerical fracture stresses and fracture strains were compared with the corresponding experimental values. The fracture stresses varied by a maximum 3% whereas the fracture strain differed by a maximum 5% when compared to the corresponding experimental values.

Table 2: Material Models for A992 and 350W Steel Grades

Steel Grade-Element	Power Model (Region IV)	Weighting Constant w (Region V)
A992 - Flange	$F_t = 860.4\ (\varepsilon_t)^{0.1411}$	w = 0.6
A992 - Web	$F_t = 942.8\ (\varepsilon_t)^{0.1611}$	w = 0.5
350W-Flange	$F_t = 905.6\ (\varepsilon_t)^{0.1511}$	w = 0.6
350W-Web	$F_t = 943.2\ (\varepsilon_t)^{0.1628}$	w = 0.5

4. Analysis of Perforated Tension Coupons

The material constitutive relations developed based on the experimental-numerical analysis of the standard coupons were used to establish the load-deformation behaviour of perforated samples. Figure 7 compares the FE results with the test results for the perforated samples obtained from the flanges and webs of the A992 steel section. As can be seen in Figure 7, the calculated (using FE models) average stress-strain responses show a reasonably good agreement with the test responses. Similar comparisons were also made on the 350W steel perforated steel tension specimens. Again, the numerical simulation agreed well with the experimental results. Table 3 summarizes the experimentally and numerically obtained ultimate strength values for the perforated coupons. As indicated in the fifth column of Table 3, the FE results varied by less than 5% when compared to the experimental results.

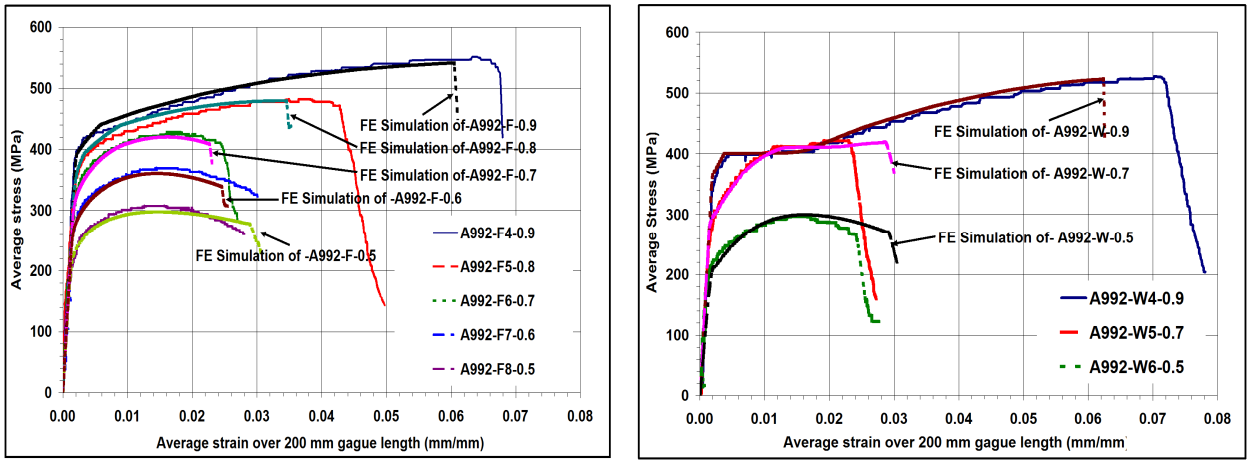

Figure 7: Analysis of Perforated Tension Coupons – A992 Steel Grade

Table 3: Comparison of Experimental Test Results with FEM Prediction for Perforated Samples

Steel Grade (1)	Specimen ID (2)	Experimental Ultimate-stress $F_u^{Exp} = \left(P_u / A_g\right)_{Exp}$ (MPa) (3)	FEM Ultimate-stress $F_u^{FEM} = \left(P_u / A_g\right)_{FEM}$ (MPa) (4)	$\left(F_u^{Exp} / F_u^{FEM}\right)$ (5)
A992	**A992-F-0.9**	547	542	1.01
	A992-F-0.8	482	480	1.00
	A992-F-0.7	429	423	1.01
	A992-F-0.6	369	362	1.02
	A992-F-0.5	308	298	1.03
	A992-W-0.9	528	523	1.01
	A992-W-0.7	422	418	1.01
	A992-W-0.5	297	299	0.99
350W	**350W-F-0.9**	548	547	1.00
	350W-F-0.8	489	488	1.00
	350W-F-0.7	427	427	1.00
	350W-F-0.6	366	366	1.00
	350W-F-0.5	311	312	1.00
	350W-W-0.9	540	543	0.99
	350W-W-0.7	417	417	1.00
	350W-W-0.5	291	302	0.96

5. Conclusions

Steel structures construction often necessitates fabrication of holes in the flanges of steel beams. A research project indicated that the beams having smaller holes failed due to flange buckling, whereas the beams having larger tension flange holes failed due to fracture. If one has to build finite element models for such studies, then such FE models require realistic material stress-strain relationships, which can capture the fracture of steel as well. This paper discussed the experimental and numerical investigations conducted on solid, as well as perforated, steel tension members to establish such material models for the behaviour of structural steel. The following observations were made during this study;

- The average yield strength of the flange coupons of the A992 steel was 4% higher than that of the 350W steel. The average ductility ratio of the A992 flange coupons was approximately 9% lower than that of 350W steel.
- The ductility of axial tension members was greatly reduced when the net section fracture strength A_nF_u was lower than the gross section yield strength A_gF_y.
- A power-law fit of experimental results in strain hardening range, and a weighted power-law $F_t = F_{ut}[w.(\varepsilon_t/\varepsilon_{ut})^n + (1\text{-}w).(1+\varepsilon_t - \varepsilon_{ut})]$ in post ultimate range can be used to derive true stress – true strain relations for steel up to fracture.
- A suitable weighting constant w can be easily obtained by employing proper FE modeling of a standard tensile coupon.
- The developed material constitutive relation based on the experimental-numerical simulation provided good load-deformation behaviour for perforated tension coupons.
- The stresses and strains at fracture for the standard coupons based on numerical analysis differed by less than 5% when compared to the corresponding results from the experiment.

6. References

ASTM Standards A370-02. (2002). Standard Test Methods and Definitions for Mechanical Testing of Steel Products, American Society for Testing and Materials, pp. 106-141.

Bathe, K.J. (1996). *Finite Element Procedures*, Prentice Hall, Englewood Cliffs, NJ, USA.

Cabezas, E.E., and Celentano, D.J. (2004). "Experimental and numerical analysis of the tensile test using sheet specimens". *Finite Elements in Analysis and Design,* 40, pp. 555-575.

Bruneau, M., Uang, C.M., and Whittaker, A. (1998). *Ductile Design of Steel Structures*, McGraw-Hill Companies, Inc, N.Y, USA.

CISC. (2007). *Handbook of Steel Construction*, Canadian Institute of Steel Construction, Willowadale, Ontario, Canada.

CSA. (2003). Limit States Design of Steel Structures, CAN/CSA-S16-01, Canadian Standard Association, ON, Canada.

Fisher, J.W., and Struik, J.H.A. (1974). Guide to Design Criteria for Bolted and Riveted Joints, John Wiley & Sons, N.Y, USA.

Hollomon, J.H. (1945). Tensile Deformation, Transaction of American Institute of Mechanical Engineering, Vol. 162, pp. 268-277.

Jaquess, K.T, and Frank, K. (1999). Characterization of the Material Properties of Rolled Sections, Report No. SAC/BD-99/07, SAC Joint Venture, USA.

Khoo, A, H. (2000). Ductile Fracture of Steel, Ph.D Thesis, University of Alberta, Alberta, Canada.

Liu, A. (2005). Mechanics and Mechanisms of Fracture, An Introduction, ASM International, Materials Park, OH, 44073-0002.

Ling, Y. (1996). "Uniaxial true stress-strain after necking". *AMP Journal of Technology*, Vol. 5, pp. 37-48.

Mackenzie, A.C, Hancock, J.W, and Brown, D.K. (1977). "On the influence of state of stress on ductile failure initiation in high strength steels". *Engineering Fracture Mechanics*, Vol.9, pp. 167-188.

Zhang, K.S, and Li, Z.H. (1994). "Numerical analysis of the stress-strain curve and fracture initiation for ductile material". *Engineering Fracture Mechanics*, Vol.49, pp. 235-241.